



저작자표시-비영리-동일조건변경허락 2.0 대한민국

이용자는 아래의 조건을 따르는 경우에 한하여 자유롭게

- 이 저작물을 복제, 배포, 전송, 전시, 공연 및 방송할 수 있습니다.
- 이차적 저작물을 작성할 수 있습니다.

다음과 같은 조건을 따라야 합니다:



저작자표시. 귀하는 원저작자를 표시하여야 합니다.



비영리. 귀하는 이 저작물을 영리 목적으로 이용할 수 없습니다.



동일조건변경허락. 귀하가 이 저작물을 개작, 변형 또는 가공했을 경우에는, 이 저작물과 동일한 이용허락조건하에서만 배포할 수 있습니다.

- 귀하는, 이 저작물의 재이용이나 배포의 경우, 이 저작물에 적용된 이용허락조건을 명확하게 나타내어야 합니다.
- 저작권자로부터 별도의 허가를 받으면 이러한 조건들은 적용되지 않습니다.

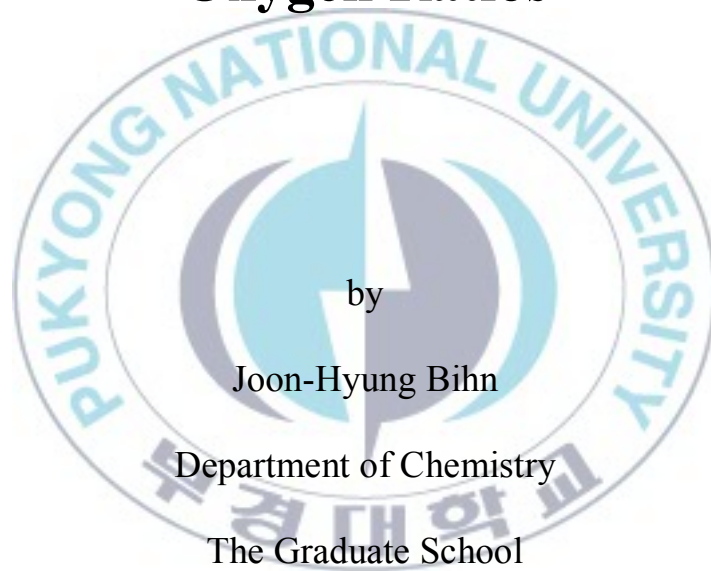
저작권법에 따른 이용자의 권리는 위의 내용에 의하여 영향을 받지 않습니다.

이것은 [이용허락규약\(Legal Code\)](#)을 이해하기 쉽게 요약한 것입니다.

[Disclaimer](#)

Thesis for the Degree of Master of Science

**Physicochemical Analysis of Mo  
Films Deposited by RF  
Magnetron Sputtering at Various  
Oxygen Ratios**



by

Joon-Hyung Bihn

Department of Chemistry

The Graduate School

Pukyong National University

February 2011

**Physicochemical Analysis of Mo Films  
Deposited by RF Magnetron Sputtering  
at Various Oxygen Ratios**

다양한 산소 조건에서 RF 마그네트론  
스퍼터링으로 합성한 Mo 산화물  
필름의 물리화학적 분석

Advisor : Prof. Yong-Cheol Kang

by

Joon-Hyung Bihn

A thesis submitted in partial fulfillment of the requirements  
for the degree of

Master of Science

in Department of Chemistry, The Graduate School,  
Pukyong National University

February 2011

Physicochemical Analysis of Mo Films Deposited by RF  
Magnetron Sputtering at Various Oxygen Ratios

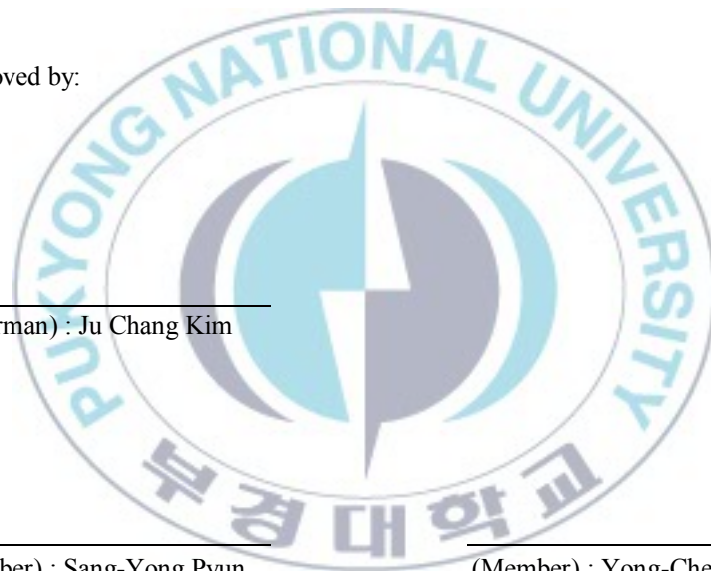
A Dissertation  
by  
Joon-Hyung Bihn

Approved by:

\_\_\_\_\_  
(Chairman) : Ju Chang Kim

\_\_\_\_\_  
(Member) : Sang-Yong Pyun

\_\_\_\_\_  
(Member) : Yong-Cheol Kang



February 2011

## CONTENTS

<b>ABSTRACT</b> .....	1
<b>CHAPTER I. Theories</b> .....	2
<b>1.1. X-ray Photoelectron Spectroscopy</b> <b>( X P S )</b> .....	2
<b>1.2. Sputtering</b> <b>Deposition</b> .....	7
<b>CHAPTER II. Physicochemical analysis of Mo films</b> <b>deposited by RF magnetron sputtering at various</b> <b>oxygen ratio</b> .....	12
<b>2.1. Introduction</b> .....	12
<b>2.2. Experimental Section</b> .....	14
<b>2.3. Results and Discussion</b> .....	18
2.3.1. XPS analysis.....	18
2.3.2. XRD analysis of Mo films.....	27
2.3.3. AFM and SEM study.....	29
2.3.4. SE investigation of Mo films.....	31
<b>2.4. Conclusion</b> .....	36
<b>2.5. References</b> .....	37
<b>KOREA ABSTRACT</b> .....	41
<b>ACKNOWLEDGEMENT</b> .....	42



## List of Figures

- Figure 1.** Process of photoelectron generation.....4
- Figure 2.** Energy relationship of  $B \cdot E$ ,  $K \cdot E$ ,  $h\nu$  and work function.....5
- Figure 3** Schematic diagram of RF-sputtering system used in this research.....11
- Figure 4.** XP spectra of Mo 3d region of Mo films obtained at different oxygen ratios in a) and representative deconvoluted Mo 3d XP spectra of MoO-0, MoO-5, and MoO-40 in b), c), and d), respectively. Note the relative intensities of b), c), and d). In the figure b) - d), Shirley background was adapted and curly lines represent raw data and the solid lines overlapped with the curly line are sum of the deconvoluted peaks.....20
- Figure 5.** XP spectra of O 1s region of Mo films obtained at different oxygen ratios in a) and representative

deconvoluted O 1s XP spectra of MoO-0, MoO-5, and MoO-40 in b), c), and d), respectively. In the figure b) - d), Shirley background was adapted and curly lines represent raw data and the solid lines overlapped with the curly line are sum of the deconvoluted peaks.....24

**Figure 6.** XP spectra of molybdenum films at valence band region. The vertical dotted lines were added for clear comparison.....26

**Figure 7.** Representative XRD patterns of molybdenum films ; MoO - 0 and MoO - 40 ..... 27

**Figure 8.** Sectional SEM views of MoO-0 and MoO-40 in a) and b), respectively and 3D-AFM images of those in c) and d), respectively. Note the z-scale in AFM images.....29

**Figure 9.** Thickness of the molybdenum films obtained from SE data by applying generation oscillation method

using Gaussian model. Thickness was measured  
several times for each film.....32

**Figure 10.** Direct band gap energies,  $E_g$ , of the molybdenum  
films.....34



## List of Tables

<b>Table 1.</b> Valence band maximum (VBM), direct band gap energy ( $E_g$ ), and the root mean square (RMS) roughness of the molybdenum films.....	35
---	----



# **Physicochemical Analysis of Mo Films Deposited by RF Magnetron Sputtering at Various Oxygen Ratios**

Joon-Hyung Bihn

Department of Chemistry, Graduate School,  
Pukyong National University

## **Abstract**

The results of deposition and physicochemical characterization of molybdenum thin films are described in this thesis. The physical and chemical properties of Mo oxide films were examined with X-ray diffraction (XRD) and X-ray photoelectron spectroscopy (XPS) techniques. The obtained Mo films at the oxygen ratio of 0% showed crystallinity of cubic Mo(110) phase. After the oxygen ratio increased more than 5% in the sputter gas, the Mo oxide films were formed as an amorphous phase. The thickness of the thin film was drastically decreased from 1000 to ca 70 nm after introduction of oxygen in the sputter gas confirmed by spectroscopic ellipsometry (SE) and scanning electron spectroscopy (SEM). The calculated band gap of the film increased from 3.17 to 3.63 eV by addition of oxygen in the sputter gas. XPS results revealed that the ratio of metallic Mo species in the Mo oxide films decreased but the contents of Mo<sup>6+</sup> species increased as the ratio of oxygen increased in the sputter gas and fully oxidized at low content of oxygen in the sputter gas.

## **CHAPTER I. Theories**

### **1.1. X-Ray Photoelectron Spectroscopy**

X-Ray Photoelectron Spectroscopy (XPS), as known as Electron Spectroscopy for Chemical Analysis (ESCA), is analytical technique for the surfaces of solid materials used to obtain chemical information. Both composition and the oxidation state of surface constituents can be determined by XPS after peak deconvolution process association of spin-orbit splitting parameter. Insulators and conductors can easily be analyzed in surface areas from a few microns to a few millimeters across with this technique.

XPS technique is based on Einstein's idea about photoelectric effect, this concept developed around 1905. The concept of photons was used to describe the ejection of electrons from a surface element when photons were impinged upon it. In principle, XP spectra of detected signals are well defined in term of the binding energy of electronic states of atoms. Photons with enough energy to eject the core electron of an element transferred their energies to electrons and electron received the energy is

ejected from the atom becoming a photoelectron. These procedures are schematically shown in Figure 1. The incident x-rays cause the ejection of core-level electrons from sample atoms. The energy of a photo emitted core electron is a function of its binding energy and is characteristic of the element from which it was emitted. Energy analysis of the emitted photoelectrons is the data used for XPS. When the core electron is ejected by the incident x-ray, an outer electron fills the core hole. The energy of this transition is balanced by the emission of an Auger electron or a characteristic x-ray. Analysis of Auger electrons can be used in XPS, in addition to emitted photoelectrons.

The photoelectrons and Auger electrons' energies are determined as a function of their velocity entering the detector. By counting the number of photoelectrons and Auger electrons as a function of their energy, a spectrum representing the surface composition is obtained. The energy corresponding to each peak is characteristic of an element present in the sampled volume. The area under a peak in the spectrum is a measure of the relative

amount of the element represented by that peak. The peak shape and precise position indicates the chemical state for the element.

Figure 1 shows brief mechanism of production of photoelectron. The incident photon ejects the electron bound in core level of atoms.

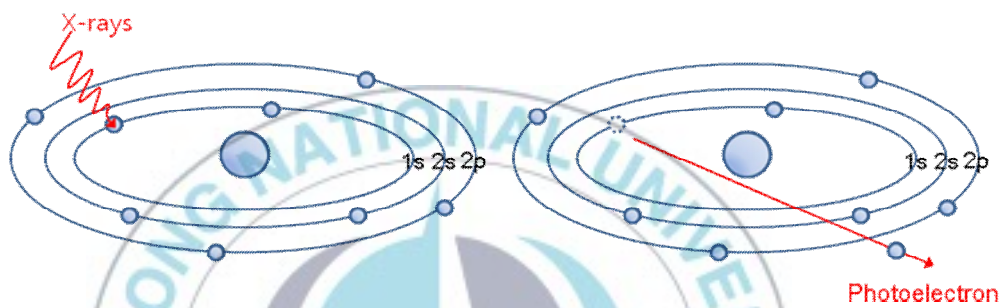


**Figure 1.** Process of photoelectron generation.

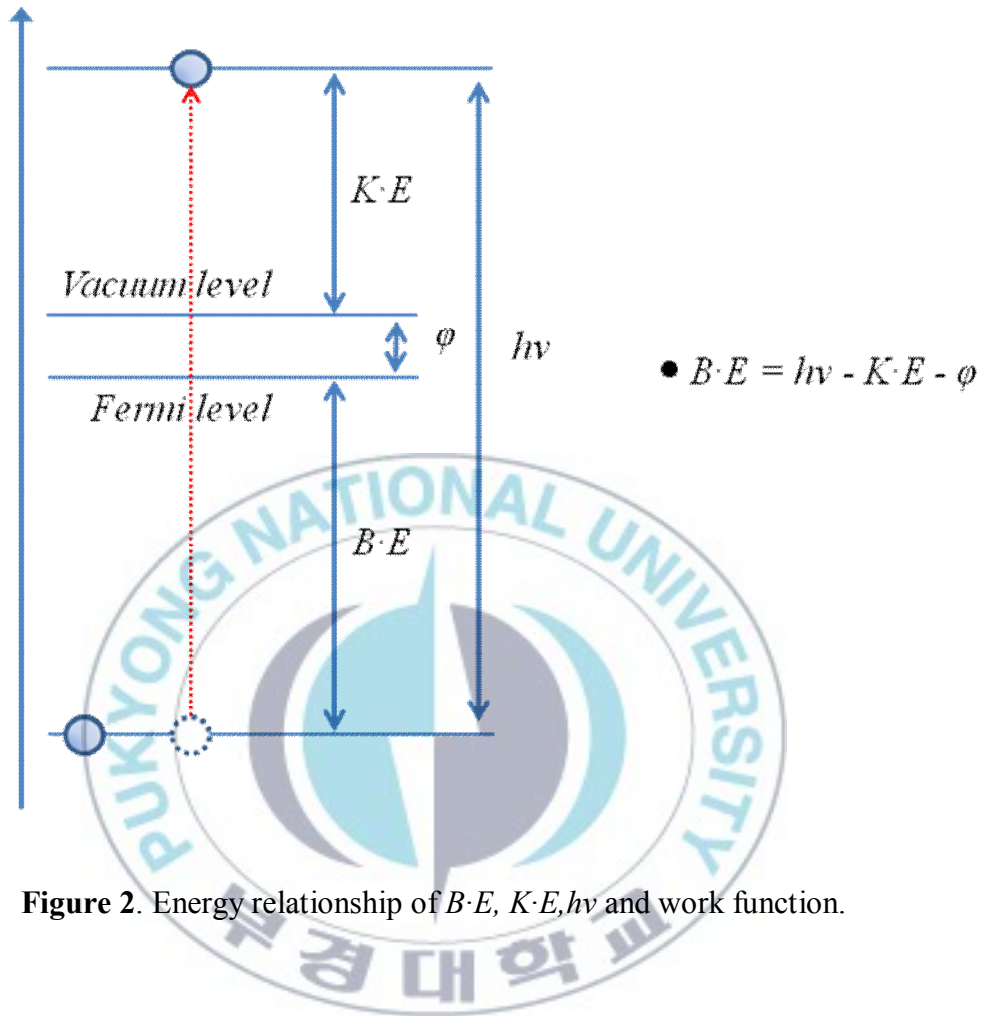


**Figure 2.** Energy relationship of  $B \cdot E$ ,  $K \cdot E$ ,  $h\nu$  and work function.

The binding energy of an electron in a certain element is unique. From the relationship of binding energy ( $B \cdot E$ ), kinetic energy of photoelectron ( $K \cdot E$ ), work function ( $\varphi$ ) of the sample,

and the photon energy shown in Figure 2, we can identify the element on the interested surface. This is the main concept of XPS analysis.



## **1.2. Sputtering Deposition**

One of the main methods used for deposition of thin films onto substrates is sputtering deposition. This technique is used for the coating of a variety of materials such as metals, semiconductors and insulators, both in an industrial and research level. A variation of this technique, the magnetron-sputter deposition, can provide better sputtering rates and higher yield by effectively utilizing and combining strong electric and magnetic fields during the sputter process. When a solid material surface is being bombarded with energetic particles (e.g. accelerated ions), a cascade of collisions takes place, causing a number of surface atoms to eject from the target material and follow random trajectories. This simple phenomenon is called sputtering.

Aside from the ejected atoms, the emission of secondary electrons from the target material also takes place. These secondary electrons are necessary in order to sustain the plasma (glow discharge phenomenon) and maintain the deposition process. Many of the techniques developed for depositing thin films take

advantage of the sputter phenomenon. The main system used by these techniques consists of a pair of planar electrodes, the anode where the substrate (e.g. silicon wafer) is placed, and the cathode (target) that is made up of the material that will be used for the thin film deposition onto the substrate. The two electrodes are located inside the low pressure vacuum deposition chamber ( $5 \times 10^{-7}$  Torr of base pressure). This is a chamber filled with the sputtering gas, usually an inert gas such as argon (Ar).

Once negative voltage is applied to the target surface, any existing Ar positive ions will accelerate towards the cathode and after falling on it, a small stream of atoms or clusters of atoms will eject from the cathode material. A small portion of them will impact on the anode's wafer, leading to the formation of a thin film onto the substrate. In order to keep the process going, constant gas ionizations are necessary and this is achieved with the aid of the secondary electrons that collide with neutral atoms and generate new ions.

The sputter yield,  $S$ , is provided by the following equation:

$$S = \frac{\textit{number of atoms removed}}{\textit{number of incident ions}}$$

And the sputter yield is highly dependent on the:

- incident ion's energy,
- target material,
- incident angle and
- target structure.

In order to increase performance, variations on the basic principle have been developed. One of the many variations involves the use of a magnetic field close to the cathode's plane. The secondary electrons generated during the sputter process are trapped by this field and stay close to the cathode surface. Following helical paths around the magnetic field lines, these electrons are forced to travel longer distances inside the chamber and thus induce more ionizations and finally increase the sputter yield,  $S$ , in a significant degree.

The use of this variation has certain advantages. It allows for an increased sputter rate, higher plasma density, and the ability to sustain plasma at lower pressure, meaning that less gas is needed in the vacuum chamber.

By modifying various parameters, it is possible to deposit almost all kinds of materials. The use of DC power supply is suitable for metal targets, while the use of RF or pulsed DC supply enables to sputter semiconductors and insulators as targets as well. Also, the use of a reactive gas instead of an inert gas (called reactive sputtering), enables the chemical reaction between the gas and the target material and thus the deposition of a compound thin film onto the substrate.

These controllable variables, make the magnetron-sputter technique very efficient compared to other deposition methods and suitable for almost every target material.

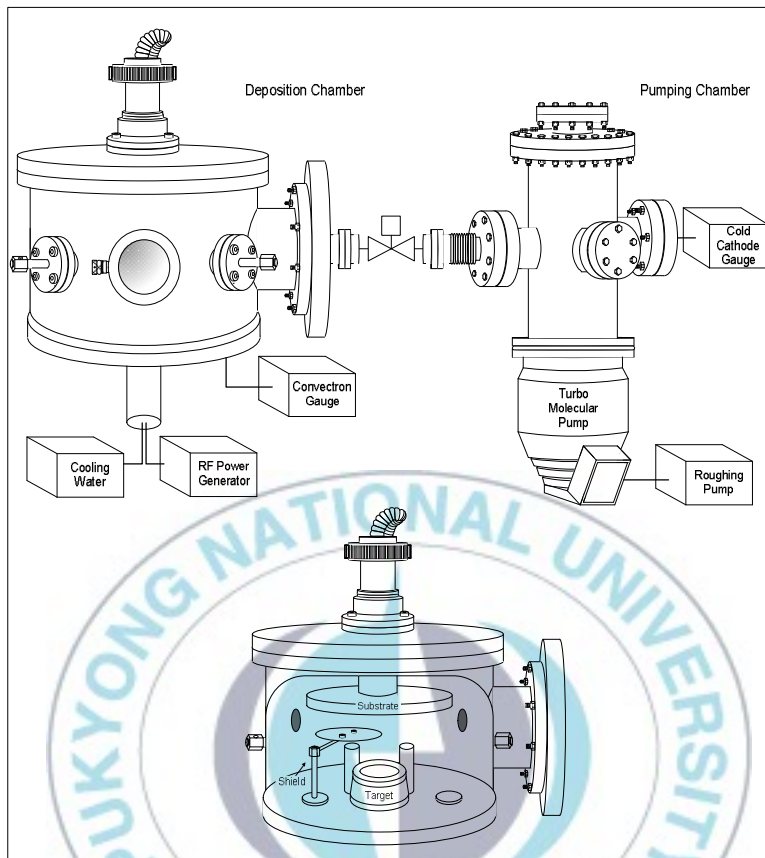


**Figure 3.** Schematic diagram of RF-sputtering system used in this research.

## **CHAPTER II. Physicochemical analysis of Mo films deposited by RF magnetron sputtering at various oxygen ratio**

### **2.1. Introduction**

Molybdenum oxides ( $\text{MoO}_x$ ) have many advantages in a wide variety of physical and chemical applications. These applications are well known as transparent conducting light-trapping oxides (TCLOs) [1], catalysis [2,3], back contact material in solar cell application of  $\text{Cu}(\text{InGa})\text{Se}_2$  (CIGS) [4,5], gas sensors [6], and electrochromic devices [7,8]. Because of these applications, many researchers have studied this material system intensively. Comini *et al.* reported the feasibility of molybdenum(VI) oxide nanorods on gas sensing especially for CO. They reported that the guaranteed stable phase of molybdenum oxide was in a crystal phase rather than in an amorphous phase. Meng *et al.* reported molybdenum doped in complex metal increased the ability of electron mobility in indium oxide film (IMO) [9].

Molybdenum(VI) oxide thin films have been synthesized

with various methods including DC reactive magnetron sputtering [10,11], laser-assisted deposition [12], spray pyrolysis [13], electron beam evaporation [14,15], thermal evaporation [16-18], and sol-gel process [19]. Controlling the band gap and the crystallinity of the films are critical for a wide range of applications including gas sensing, TCLOs, CIGS, and display devices.

In this work, molybdenum oxide and/or oxyhydroxide was fabricated by applying the RF reactive sputtering method at various oxygen gas ratios in the sputtering gas to manipulate the electronic and physical structure of the molybdenum oxide and/or oxyhydroxide films. The effect of oxygen ratio in the sputtering gas on the morphology, crystallinity, and roughness of the molybdenum films was examined. Also the detailed oxidation states of Mo 3d and O 1s and direct band gap energies of the Mo films were investigated as well.

## 2.2. Experimental Section

Molybdenum (99.95%, Tasco) target with 5 mm of thickness and 50 mm of diameter was used in radio frequency (RF) magnetron sputtering for Mo films. High purity argon (99.99%) and oxygen (99.99%) gases were used for sputtering and reactive gas, respectively. The p-type Si(100) wafer was used as a substrate after cleaning with 2% HF solution and drying with nitrogen gas by the known cleaning method [20]. The deposition chamber was evacuated to the base pressure of  $1.0 \times 10^{-7}$  Torr using a roughing pump and a turbo molecular pump. The flow rates of argon and oxygen were adjusted by mass flow controllers separately. The molybdenum target was pre-sputtered for 1 hr at the power of 30 W for cleaning and stabilizing the plasma with the blended sputtering gases while the target was shielded. Then molybdenum was sputtered on the substrate at room temperature after pre-sputtering treatment with various oxygen ratios ( $O_2 / O_2 + Ar$ ) to form Mo thin films. In this work, the total sputtering gas flow rate was kept at 20 sccm and the working pressure of the

sputtering chamber during the RF sputtering process was maintained at  $48 \pm 1$  mTorr measured with a convectron gauge.

Field emission scanning electron microscopy (FESEM, JEOL JSM-6700F, Japan) images were taken with the high voltage of 15 kV and the beam current of 9 ~ 10 mA to verify the thickness of molybdenum films. The obtained Mo films were mounted on a sample holder after coating with OsO<sub>4</sub>. The surface morphology of the Mo films was analyzed by atomic force microscopy (AFM, Veeco Multimode Digital Instruments Nanoscope IIIa, USA) applying contact mode. The scan rate and the tip velocity applied in this work were 1.97 Hz and 7.88  $\mu\text{m/s}$ , respectively. AFM images of the films were collected in the area of  $2 \times 2 \mu\text{m}^2$  and the roughness of the film was determined in root mean square (RMS) values. The crystal structure of the films was examined with X-ray diffraction (XRD, PHILIPS X'Pert-MPD, Netherland) system applying a grazing mode with Cu K $\alpha$  ( $\lambda = 1.5406 \text{ \AA}$ ) radiation with  $0.02^\circ$  step size.

The optical parameters such as the refractive index and the extinction coefficient of Mo films were measured by spectroscopic ellipsometry (SE, J.A.Woollam M-2000D, USA). The D<sub>2</sub> and quartz tungsten halogen lamps were used as the source of ellipsometer in the wavelength range from 193 to 1000 nm. The beam size and incident angle were 2 mm and 75°, respectively. Generation oscillation method using Gaussian model was applied to calculate the thickness of Mo oxide films.

The compositional analyses of Mo films were carried with X-ray photoelectron spectroscopy (XPS, VG MultiLab 2000, UK), using a monochromatic Al K $\alpha$  (1486.6 eV) X-ray source. The base pressure in the XPS chamber was kept at  $1 \times 10^{-10}$  Torr. The X-ray source was created at the power of 24 kW and the beam current was 16.5 mA. The survey XP spectra were collected with a concentric hemispherical analyzer (CHA) in constant analyzer energy (CAE) mode with the pass energy of 50 eV, a dwell time of 50 ms, and an energy step size of 0.5 eV. The binding energy (BE) scale was corrected by referring to the aliphatic C 1s at 284.6

eV for consistency. [21] High resolution XP spectra (Mo 3d, O 1s, and valence band) were obtained at the pass energy of 20 eV, an energy step size of 0.02 eV, and other factors were kept the same as those applied in the survey scan. The detailed parameters are described elsewhere. [21,22]



## 2.3. Results and Discussion

### 2.3.1. XPS analysis

The chemical nature of the Mo films deposited at different O<sub>2</sub> ratios was studied with X-ray photoelectron spectroscopy (XPS). The high resolution Mo 3d XP spectra of the Mo films are shown in Figure 4. The doublet Mo 3d feature in the XP spectra of MoO-0 was ill-defined and shifted to higher binding energy after increasing the O<sub>2</sub> ratio. In order to get more detailed information about the oxidation state of Mo, deconvolution of Mo 3d peaks was performed with the XPSPEAK program with spin-orbit splitting (SOS) constant of 3.15 eV. The deconvoluted peaks of Mo 3d range of MoO-0, MoO-5, and MoO-40 are shown in Figure 4 b), c), and d), respectively.

Four different oxidation states of Mo were assigned in MoO-0 after deconvolution and only Mo(VI) state was detected in MoO-5 and MoO-40 films. The assigned binding energies of different

Mo  $3d_{5/2}$  in MoO-0 are centered at 228.3, 228.9, 231.8, and 232.9 eV for Mo(0), Mo(IV), Mo(V), and Mo(VI), respectively. These assigned binding energies are consistent with the reported values [23-25]. Although oxygen was not supplied during the RF sputtering, partially and fully oxidized Mo species were mixed with Mo(0) species in MoO-0 film shown in Figure 4 b).



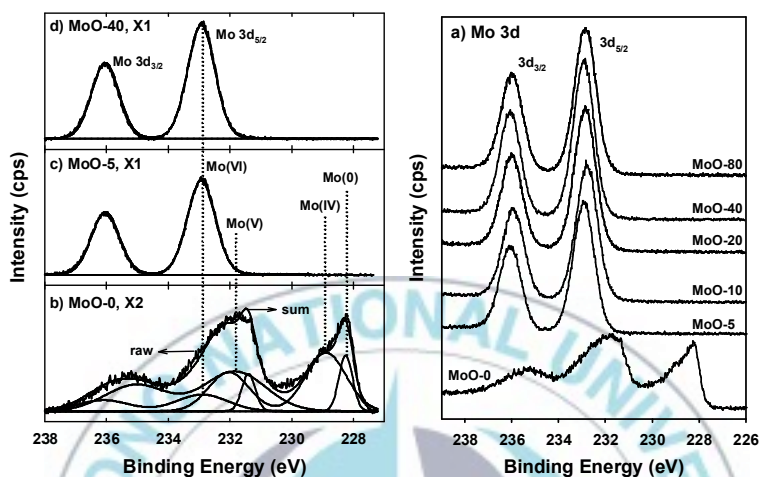


**Figure 4.** XP spectra of Mo 3d region of Mo films obtained at different oxygen ratios in a) and representative deconvoluted Mo 3d XP spectra of MoO-0, MoO-5, and MoO-40 in b), c), and d), respectively. Note the relative intensities of b), c), and d). In the figure b) - d), Shirley background was adapted and curly lines represent raw data and the solid lines overlapped with the curly line are sum of the deconvoluted peaks.

This may be explained through the residual oxygen moieties, such as water and hydroxyl group, in the sputtering chamber which participated on the formation of molybdenum oxide and/or molybdenum oxyhydroxides ( $\text{MoO}(\text{OH})_2$ ,  $\text{Mo}(\text{OH})_4$  for Mo(IV) and  $\text{MoO}(\text{OH})_4$ ,  $\text{MoO}_2(\text{OH})_2$  for Mo(VI) etc.). When the  $\text{O}_2$  ratio was increased to 5% in the sputtering gas, only the Mo(VI) species was detected and the other states were not observed (Figure 4 c). This implies that Mo species were fully oxidized even at low content of oxygen. To verify the gradual oxidation process of Mo as a function of  $\text{O}_2$  ratio, more prudent control of the ratio of  $\text{O}_2$  gas is crucial. Unfortunately, the RF deposition chamber used in this work was not equipped with a high precision mass flow controller. Further increase of  $\text{O}_2$  ratio did not affect the oxidation state of Mo shown in Figure 4 d), which is added for clear comparison with MoO-5.

In high resolution XP spectra of O 1s (Figure 5a) of Mo films, apparent peak shift, about 0.27 eV, was observed by increasing  $\text{O}_2$  ratio. After the deconvolution process of the O 1s region, three oxygen species were assigned as  $\text{O}^{2-}$ ,  $\text{OH}^-$ , and  $\text{H}_2\text{O}$

centered at 530.9, 531.5, and 532.8 eV [26], respectively. The surface oxygen, denoted as H<sub>2</sub>O in the figure, existed at almost constant level by increasing the O<sub>2</sub> ratio. The ratio of OH<sup>-</sup> to O<sup>2-</sup> was converted from 1.63 of MoO-0 to 0.38 of MoO-40 after Mo species were oxidized to Mo(VI). The fact that Mo species were oxidized was confirmed in Mo 3d XP result. A plausible oxidation mechanism of Mo species based on the Mo 3d and O 1s XPS results could be proposed as followings.



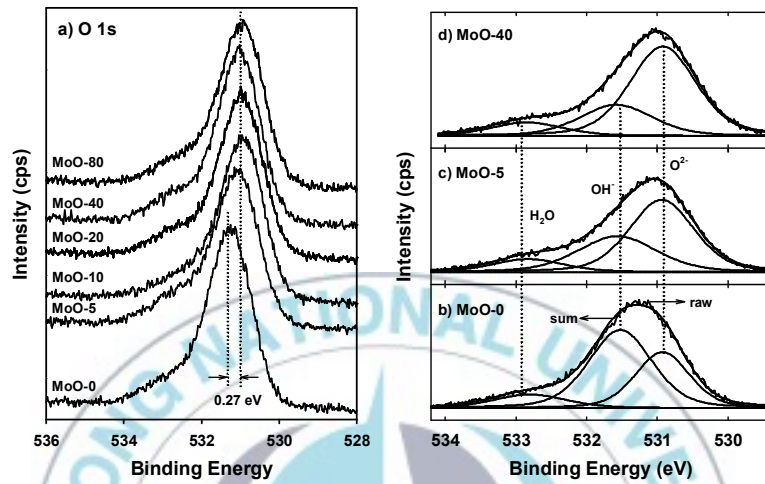


**Figure 5.** XP spectra of O 1s region of Mo films obtained at different oxygen ratios in a) and representative deconvoluted O 1s XP spectra of MoO-0, MoO-5, and MoO-40 in b), c), and d), respectively. In the figure b) - d), Shirley background was adapted and curly lines represent raw data and the solid lines overlapped with the curly line are sum of the deconvoluted peaks.

The Mo(IV) species ( $\text{MoO}_2$ ,  $\text{MoO}(\text{OH})_2$ ,  $\text{Mo}(\text{OH})_4$ ) and Mo(V) species ( $\text{Mo}_2\text{O}_5$ ,  $\text{MoO}(\text{OH})_3$ ,  $\text{MoO}_2(\text{OH})$ ) were oxidized to  $\text{MoO}_3$  by increasing  $\text{O}_2$  content. Therefore the intensity of  $\text{O}^{2-}$  increased and that of  $\text{OH}^-$  decreased by the oxidation of Mo from Mo(IV,V) to Mo(VI) moiety.

The valence band spectra of MoO-0 evolved by Mo 4d and O 2p centered at  $\sim 2$  and  $\sim 7$  eV [27] below Fermi level, respectively, are shown in Figure 6. When the  $\text{O}_2$  ratio increased, the density of state (DOS) of Mo 4d vanished and that of O 2p increased. The total DOS was reduced by diminishing the DOS of Mo 4d after oxygen was introduced. This implies that metallic Mo was oxidized by adding  $\text{O}_2$  which is consistent with the XPS results of Mo 3d and O 1s. The valence band maxima (VBM) of Mo films were calculated by extrapolating the line obtained by the linear square method with the linear portion near Fermi level to the constant photoemission line. The VBM of MoO-0 was -0.44 eV then shifted to higher binding energy at  $3.07 \pm 0.09$  eV after introducing  $\text{O}_2$ . This result shows agreement with the propensity

of band gap energy shifting observed in SE measurement. The VBM values for each Mo oxide films are presented in Table 1.



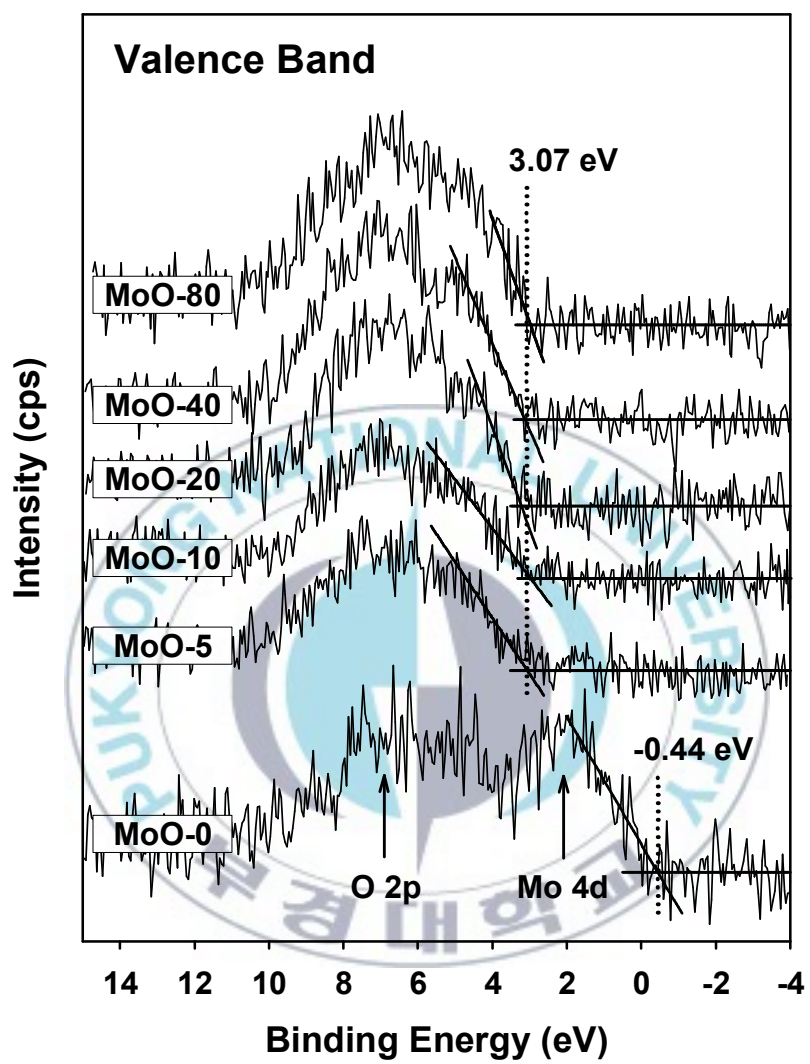


**Figure 6.** XP spectra of molybdenum films at valence band region. The vertical dotted lines were added for clear comparison.

### 2.3.2. XRD analysis of Mo films

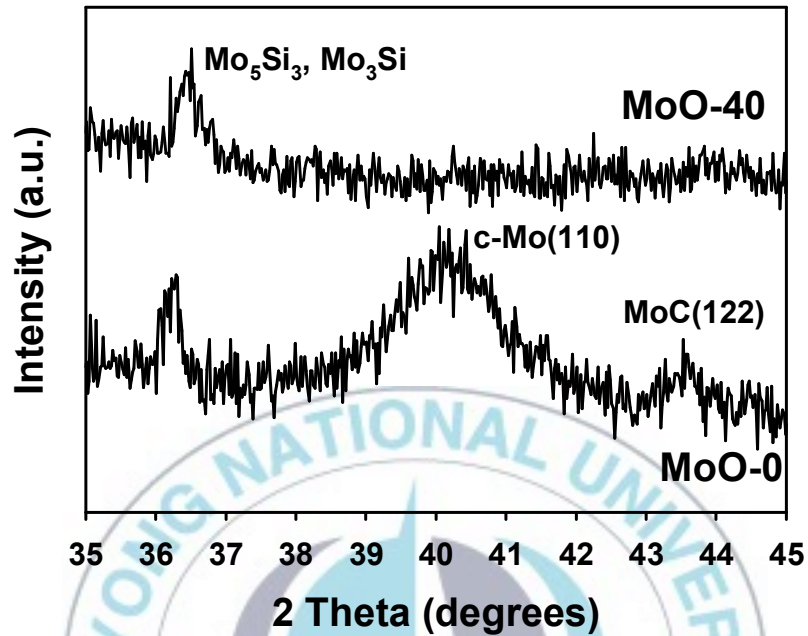
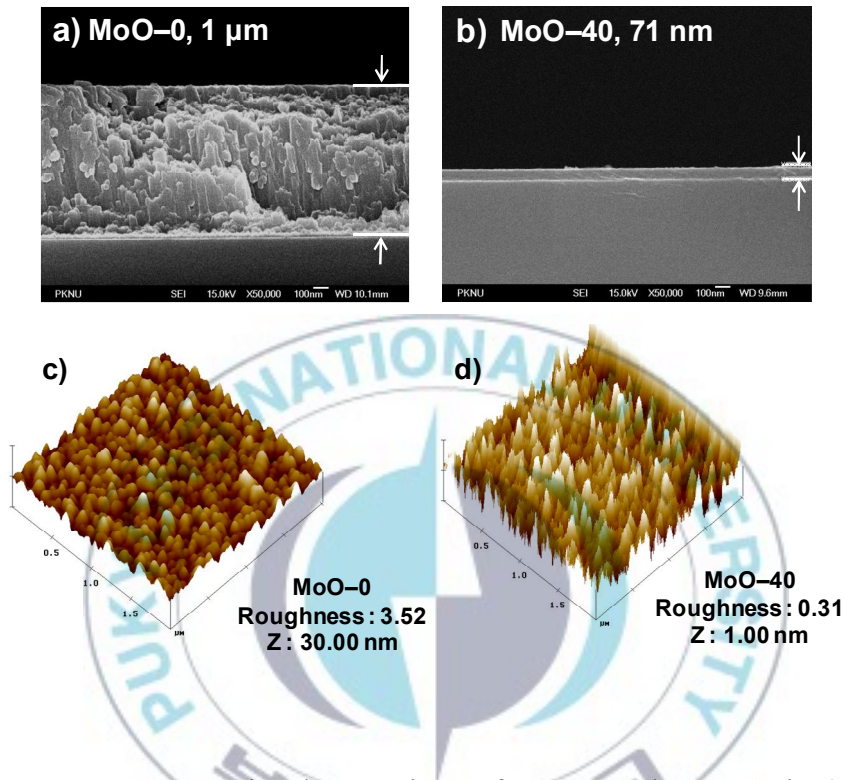


Figure 7. Representative XRD patterns of molybdenum films; MoO-0 and MoO-40.

The XRD patterns of Mo films deposited at 0 and 40% oxygen ratio in the sputtering gas are shown in Figure 7. The Mo film obtained at 40% O<sub>2</sub> is denoted as MoO-40. Molybdenum films deposited at more than 5% of O<sub>2</sub> had the same crystallinity

as that was confirmed in MoO-40. The peak detected at  $36.5^\circ$  was contributed by molybdenum silicon ( $\text{Mo}_5\text{Si}_3(002)$  or  $\text{Mo}_3\text{Si}(200)$ ). [28] The peak with low intensity at  $43.6^\circ$  was assigned to  $\text{Mo}_2\text{C}(122)$  which may be formed from the residual carbon as contaminants in the RF sputtering chamber during deposition of Mo. The MoO-0 showed c-Mo(110) phase with the average size of 5.37 nm. The size of metallic Mo crystal in MoO-0,  $L$ , was calculated by using Scherrer's equation [29] given as  $L = (a\lambda)/(H \cos \theta)$ , where  $a$  is 0.9 as the Scherrer's constant,  $\lambda$  is the wavelength of the X-ray ( $1.5406 \text{ \AA}$ ),  $H$  is the full width at half maximum of c-Mo(110) peak, and  $\theta$  is the Bragg angle. In comparison XRD data of MoO-0 with XPS results, most Mo species formed as Mo oxide which was amorphous phase. As the oxygen ratio increased, metallic cubic molybdenum phase disappeared because of the formation of molybdenum oxide and/or molybdenum oxyhydroxide in amorphous phase without any crystallinities.

### 2.3.3. AFM and SEM Study



**Figure 8.** Sectional SEM views of MoO-0 and MoO-40 in a) and b), respectively and 3D-AFM images of those in c) and d), respectively. Note the z-scale in AFM images.

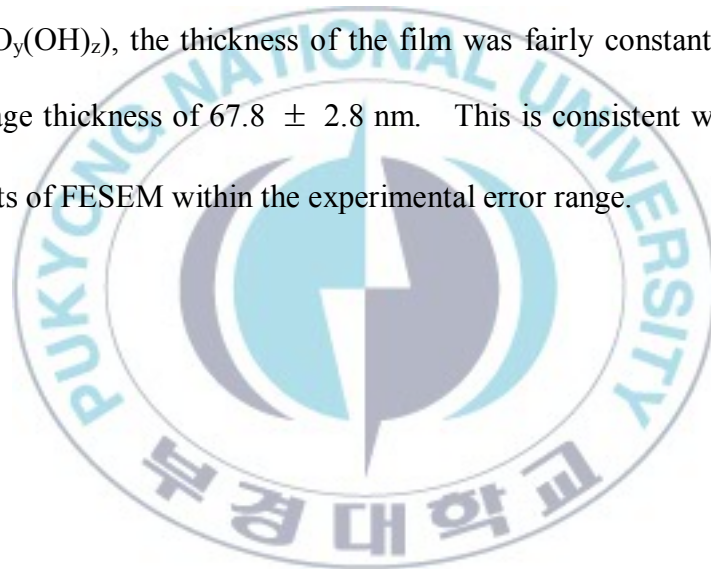
The thickness and roughness of the Mo films were examined by FESEM and AFM, respectively. Sectional FESEM

images of the MoO-0 and MoO-40 films are shown in Figure 8 a) and b), respectively. The film thickness, which was determined by the Motic Image analysis program, dramatically decreased from 1000 to 71 nm after 40% of oxygen introduced. The decreasing phenomenon of the film thickness by increasing the O<sub>2</sub> ratio agrees with the previous results of Anderle's group. [30] They have reported that the ratio of Ar in the sputtering gas controlled the sputter yield of the target. Argon acted as a sputter gas and oxygen acted as a reactive gas in the plasma. The higher the ratio of O<sub>2</sub> in the sputtering gas, the smaller the sputter yield was observed. Therefore this makes thinner molybdenum oxide and/or oxyhydroxide films deposited at higher O<sub>2</sub> ratio. Figure 8 c) and d) show 3-D AFM images of MoO-0 and MoO-40, respectively. Note the z-scale of each image. The roughness of the film after increasing oxygen ratio decreased more than ten times comparing to that of MoO-0. When the film was rough, the oxygen could easily diffuse into the film and formed molybdenum oxide/oxyhydroxide. After the diffusion of oxygen, the roughness of the film became smaller. The roughness of the

obtained Mo films is summarized in Table 1.

#### 2.3.4. SE investigation of Mo films

To confirm the thickness of the Mo films, spectroscopic ellipsometry (SE) was performed and the thicknesses of the films obtained at various oxygen ratio are depicted in Figure 9. After the formation of Mo oxide ( $\text{MoO}_x$ ) and/or oxyhydroxide ( $\text{MoO}_y(\text{OH})_z$ ), the thickness of the film was fairly constant at the average thickness of  $67.8 \pm 2.8$  nm. This is consistent with the results of FESEM within the experimental error range.



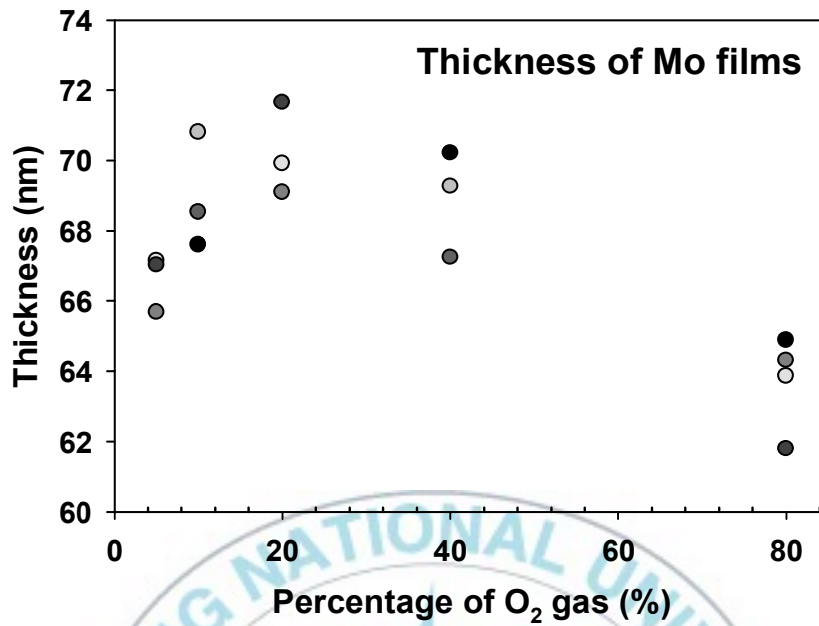


**Figure 9.** Thickness of the molybdenum films obtained from SE data by applying generation oscillation method using Gaussian model. Thickness was measured several times for each film. Direct band gap of the Mo films were calculated from the obtained SE parameters. Notably, the absorption coefficient ( $\alpha$ ) was calculated from the extinction coefficient ( $k$ ) at 1.24 ~ 6.48 eV of the photon energy by the following equation,  $\alpha = (4\pi k) / \lambda$  [31,32]. The resulted absorption coefficient was used to calculate the band gap of molybdenum films deposited at different O<sub>2</sub> gas

ratio using the following relationship,  $\alpha hv = A(hv - E_g)^m$ , where  $A$  is a constant obtained from the function of refractive index of the materials, reduced mass, and speed of light,  $hv$  is photon energy, and  $E_g$  is a band gap energy. The direct or indirect transition was determined by  $m$  value, 1/2 or 2, respectively [31,32]. In this study, the direct band gap energy ( $m = 1/2$ ) was obtained from the intersection of the extrapolating line of the linear portion in the range of 3.9 ~ 4.9 eV and the axis of the photon energy in the plots of photon energy vs.  $(\alpha hv)^2$ . The extrapolating line was obtained by the least square method and represented as dotted lines in the Figure 10. After increasing the O<sub>2</sub> ratio to 80%, the  $E_g$  increased to 3.63 from 3.17 eV of MoO<sub>3</sub>. Elangovan *et al.* reported that the band gap of Mo doped indium ranged from 3.75 (without O<sub>2</sub>) to 3.90 eV (3.5% O<sub>2</sub>) during RF sputtering depending on sputtering time and power [33]. Patil *et al.* reported that the band gap of MoO<sub>3</sub> lied in the range of 2.64 ~ 2.83 eV depending upon annealing condition and deposition time of the film [34].

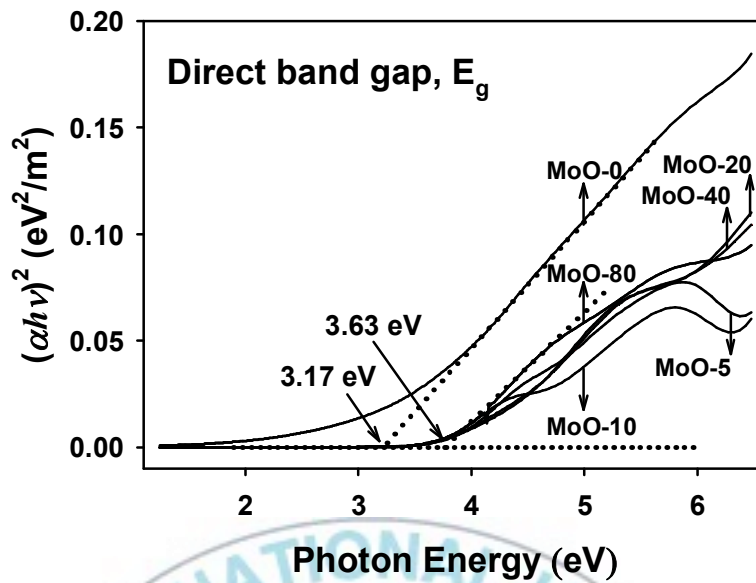


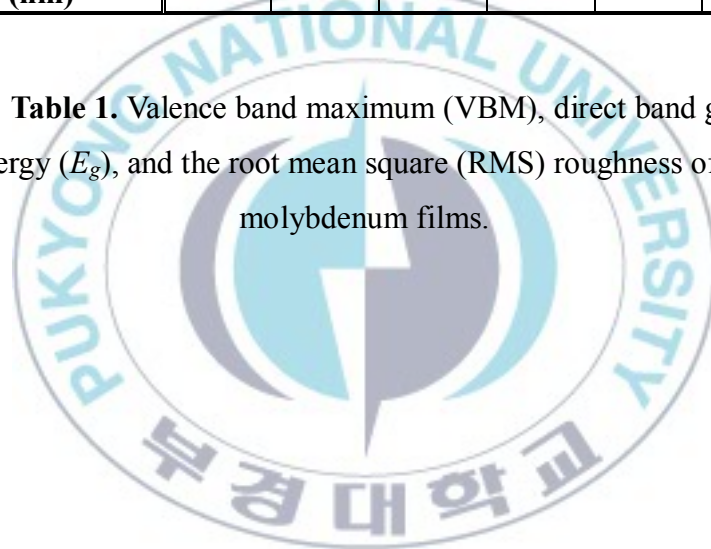
**Figure 10.** Direct band gap energies,  $E_g$ , of the molybdenum films.

The band gap obtained in this work lies in between Patil's and Elangovan's results. For clarity, the band gap energies of other films are summarized in Table 1 instead of showing in the figure. As we noticed, the direct band gap energy increased from 3.17 eV of MoO-0 to  $3.68 \pm 0.05$  eV of Mo films deposited at more than 5%  $O_2$  and stayed at almost constant level. This propensity of band gap energy increasing is consistent with the

results that the resistance of metal oxide films increased by the presence of oxidizing gases. [35]

<b>O<sub>2</sub> (%)</b>	<b>0</b>	<b>5</b>	<b>10</b>	<b>20</b>	<b>40</b>	<b>80</b>
<b>VBM (eV)</b>	<b>- 0.44</b>	<b>3.06</b>	<b>2.97</b>	<b>3.22</b>	<b>3.12</b>	<b>2.98</b>
<b>E<sub>g</sub> (eV)</b>	<b>3.17</b>	<b>3.68</b>	<b>3.63</b>	<b>3.74</b>	<b>3.73</b>	<b>3.63</b>
<b>Roughness (nm)</b>	<b>3.52</b>	<b>0.18</b>	<b>0.18</b>	<b>0.43</b>	<b>0.31</b>	<b>0.20</b>

**Table 1.** Valence band maximum (VBM), direct band gap energy ( $E_g$ ), and the root mean square (RMS) roughness of the molybdenum films.



## 2.4. Conclusions

Molybdenum films were deposited at various oxygen ratios in the sputtering gas on p-type Si(100) wafer by RF magnetron sputtering method using a metallic Mo target (purity 99.95%) successfully. The XRD study revealed that only MoO-0 showed crystallinity of cubic Mo(110) phase. After the oxygen ratio increased more than 5% in the sputtering gas, the molybdenum oxide and/or oxyhydroxide films were formed as amorphous phase. The thickness of the thin film decreased from ca. 1000 nm of MoO-0 to  $67.8 \pm 2.8$  nm of the Mo films obtained after introduction of oxygen in the sputtering gas confirmed by SE and SEM. The direct band gap energy of the film changed from 3.17 to  $3.68 \pm 0.05$  eV because VBM increased after adding oxygen in the sputtering gas. XPS results revealed that the ratio of metallic Mo species in the film decreased but the contents of Mo(VI) species increased as the ratio of oxygen increased in the sputtering gas.

## 2.5. References

- [1] J.A. Anna Selvan, A.E. Delahoy, S. Guo, Y.-M. Li, Sol. Energy Mater. Sol. C 90 (2006) 3371.
- [2] R.B. Watson, U.S. Ozkan, J. Catal. 208 (2002) 124.
- [3] W. Li, S. Zhao, B. Qi, Y. Du, X. Wang, M. Huo, Appl. Catal. B: Environ. 92 (2009) 333.
- [4] M.C.K. Tinone, T. Haga, H. Kinoshita, J. Elec. Spectros. Relat. Phen. 80 (1996) 461.
- [5] N. Miyata, S. Akiyoshi, J. Appl. Phys. 58 (1985) 1651.
- [6] E. Comini, L. Yubao, Y. Brando, G. Sberveglieri, Chem. Phys. Lett. 407 (2005) 368.
- [7] T.S. Sian, G.B. Reddy, J. Appl. Phys. 98 (2005) 026104.
- [8] T. He, J. Yao, J. Photochem. Photobiol. C: Photochem. Rev. 4 (2003) 125.
- [9] Y. Meng, X.-L. Yang, H.-X. Chen, J. Shen, Y.-M. Jiang, Z.-J. Zhang, Z.-Y. Hua, J. Vac. Sci. Technol. A 20 (2001) 288.
- [10] C.V. Ramana, V.V. Atuchin, V.G. Kesler, V.A. Kochubey, L.D. Pokrovsky, V. Shutthanandhan, U. Becker, R.D. Ewing, Appl. Surf. Sci. 253 (2007) 5368.

- [11] S.H. Mohamed, S.Venkataraj, Vacuum 81 (2007) 636.
- [12] J. Torres, J.E. Alfonso, L.D. López-Carreño, Phys. Stat. Sol. C 2 (2005) 3726.
- [13] L. Boudaoud, N. Benramdane, R. Desfeux, B. Khelifa, C. Mathieu, Catal. Today 113 (2006) 230.
- [14] R. Sivakumar, M. Jayachandran, C. Sanjeeviraja, Surf. Eng. 20 (2004) 385.
- [15] V.K. Sabhapathi, O.M. Hussian, S. Uthanna, B.S. Naidu, P.J. Reddy, C. Julien, M. Balkanski, Mater. Sci. Eng. B 32 (1995) 93.
- [16] T.S. Sian, G.B. Reddy, Sol. Energy Mater. Sol. Cells 82 (2004) 375.
- [17] S.F. Durrant, B.C. Trasferetti, J. Scarmínio, C.U. Davanzo, F.P.M. Rouxinol, R.V. Gelamo, M.A. Bica de Moraes, Thin Solid Films 516 (2008) 789.
- [18] C.-S. Hsu, C.-C. Chan, H.-T. Huang, C.-H. Peng, W.-C. Hsu, Thin Solid Films 516 (2008) 4839.
- [19] K. Galatsis, Y.X. Li, W. Wlodarski, K.Kalantar-Zadesh, Sens. Actuators B 77 (2001) 478.
- [20] C.Y. Ma, F. Lapostolle, P. Briois, Q.Y. Zhang, Appl. Surf. Sci.

253 (2007) 8718.

[21] M.S. Chun, M.-J. Moon, J.Y. Park, Y.C. Kang, Bull. Korean Chem. Soc. 30 (2009) 2729.

[22] J.Y. Park, J.K. Heo, Y.C. Kang, Bull. Korean Chem. Soc. 31 (2010) 397.

[23] Z. song, T. Cai, Z. Chang, G. Liu, J.A. Rodriguez, J. Hrbek, J. Am. Chem. Soc. 125 (2003) 8059.

[24] J.S.J. Hargreaves, R.F. Howe, D. Mckay, E. Morrison, J.L. Rico, M. Stockenhuber, Top. Catal. 52 (2009) 1559.

[25] W. Grunert, A.Y. Stakheev, R. Feldhaus, K. Andres, E.S. Shpiro, K.M. Minachev, J. Phys. Chem. 95 (1991) 1323.

[26] D. Kim, S.V. Kagwade, C.R. Clayton, Surf. Interf. Anal. 26 (1998) 155.

[27] D.O. Scanlon, G.W. Watson, D.J. Payne, G.R. Atkinson, R.G. Egdell, D.S.L. Law, J. Phys. Chem. C 114 (2010) 4636.

[28] JCPDS #76-1578 and #76-1577.

[29] D.-M. Smilgies, J. Appl. Cryst. 42 (2009) 1030.

[30] G. Gottardi, N. Laidani, V. Micheli, R. Bartali, M. Anderle, Surf. Coat. Technol. 202 (2008) 2332.

- [31] F. Yakuphanoglu, A. Cukurovali, İ. Yilmaz, *Opt. Mat.* 27 (2005) 1363.
- [32] T.E. Şenadim, H. Kavak, R. Esen, *Chin. Phys. Lett.* 24 (2007) 3477.
- [33] E. Elangovan, A. Marques, A.S. Viana, R. Martins, E. Fortunato, *Thin Solid Films* 516 (2008) 1359.
- [34] R.S. Patil, M.D. Uplane, P.S. Patil, *Appl. Surf. Sci.* 252 (2006) 8050.
- [35] E. Comini, G. Faglia, G. Sberveglieri, C. Cantalini, M. Passacantando, S. Santucci, Y. Li, W. Wlodarski, W. Qu, *Sens. Actuator B* 68 (2000) 168.



## KOREA ABSTRACT

### 다양한 산소조건에서 RF 마그네트론 스퍼터링으로 합성한 Mo 산화물 필름의 물리화학적 분석

빈 준 형

Department of Chemistry, Graduate School,  
Pukyong National University

#### Abstract

이 논문에서 몰리브덴 박막의 증착된 결과와 물리화학적 특성을 설명하고자 한다. 몰리브덴 산화물 필름의 물리적 그리고 화학적 특징은 X-ray diffraction (XRD) 와 X-ray photoelectron spectroscopy (XPS)로 실험하였다.

산소 비율이 0%인 Mo 필름은 cubic Mo(110)의 결정성을 보였고 후에 산소의 비율이 스퍼터 가스에서 5%이상 증가하자 몰리브덴 필름은 무결정성 상태를 보였다. 스퍼터 가스에 산소가 도입되자 극적으로 박막의 두께는 1000 nm 에서 70 nm 로 줄었으며 이는 spectroscopic ellipsometry (SE) and scanning electron spectroscopy (SEM) 으로 확인을 하였다. 필름의 계산된 밴드갭은 스퍼터 가스에 산소를 첨가함에 따라 3.17 에서 3.63 으로 증가하였다. XPS 결과에서는 스퍼터 가스에 산소비율이 증가함에 따라 금속 몰리브덴의 비율은 감소하고 6 가 몰리브덴은 증가하였다 그리고 낮은 비율의 산소조건 하에서도 충분히 산화되었다.

## ACKNOWLEDGEMENT

많은 방황과 철부지 없는 행동에도 항상 바른 길로 인도해 주신 지도교수님 강용철 교수님께 제일 감사드리며 저의 졸업 논문을 심사해주시고 항상 곁에서 조언을 아끼지 않으신 김주창 교수님과 변상용 교수님께 말로 표현 할 수 없는 감사 드립니다.

제 실험과 논문에 많은 도움을 주고 항상 같이 동고동락한 표면분석연구실의 박주연, 황아름, 백정하에게 고마움을 전합니다.

그리고 항상 곁에서 저의 모자람을 미소와 사랑으로 감싸주신 부모님과 든든하게 옆을 지켜준 친구와 선후배들에게도 감사를 전합니다.

